Exploring and Evaluating Image Restoration Potential in Dynamic Scenes – Supplementary Material

Cheng Zhang, Shaolin Su, Yu Zhu, Qingsen Yan, Jinqiu Sun, Yanning Zhang

In this supplementary, we show more details about the DS-IRP dataset, the proposed model and more experimental results.

1. Details of the DS-IRP Dataset

In this section, we give detailed descriptions on how images in the DS-IRP dataset are generated and present more analysis and examples on generated IRP labels.

1.1. Dynamic Imaging

Due to limited page, in the main paper, we did not give detailed explanations on how images with dynamic motions are generated. In the following, we explain this process in detail.

During the exposure time Δt, we assume that the motion m_t and scene radiance ϕ_t changes accordingly from m_{t_0} and ϕ_{t_0}. Similar to [1], a scale ratio r is used to substitute for exposure time Δt, being inversely proportional to Δt, and is sampled discretely from $[1, 75]$. As a result, the motion information and scene radiance at time t under exposure time Δt can be expressed as:

$$m_t = \frac{m_{t_0}}{r}, \phi_t = \frac{\phi_{t_0}}{r} \tag{1}$$

In Figure 1, we show the generated dynamic imaging results with respect to 11 sampled r under an example scene. The ground truth image is also presented.

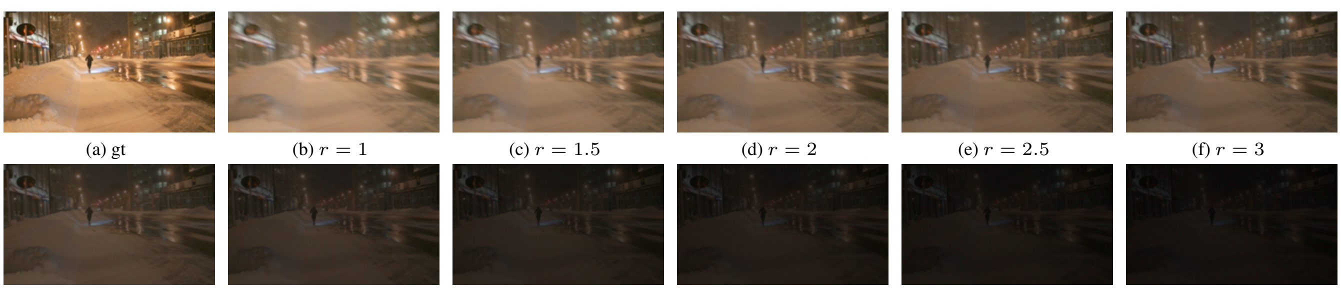

(a) gt (b) $r = 1$ (c) $r = 1.5$ (d) $r = 2$ (e) $r = 2.5$ (f) $r = 3$

(g) $r = 5$ (h) $r = 10$ (i) $r = 20$ (j) $r = 30$ (k) $r = 50$ (l) $r = 75$

Figure 1. The images with different ratios of a scene

Table 1. SRCC between IRP values generated by arbitrary two restoration models and the final averaged IRP label.

	IRP_Unet	IRP_MIR	IRP_MPR	IRP_HINet	IRP_average
IRP_Unet	-	0.9813	0.9497	0.9619	0.9884
IRP_MIR	0.9813	-	0.9414	0.9509	0.9837
IRP_MPR	0.9497	0.9414	-	0.9930	0.9827
IRP_HINet	0.9619	0.9509	0.9930	-	0.9888
IRP_average	0.9884	0.9837	0.9827	0.9888	-

1.2. IRP Labels

In the main paper, we plotted IRP values to show that the relative IRP values are slightly influenced by concrete restoration approaches. In this part, we show the IRP correlations between all the four selected restoration models [2, 5, 7, 8]. We also show their correlations to the final averaged IRP label in Table 1. It can be seen that the results in Table 1 keep high correlations, all overring 0.94 SRCC. Moreover, the correlation between four restoration models and the averaged IRP value all reached over 0.98 SRCC, indicating the reliability of the final IRP labels.

We also show more IRP values generated by four restoration algorithms under different scenes, as plotted in Figure 2. The IRP values keep consistent changes among different restoration models.

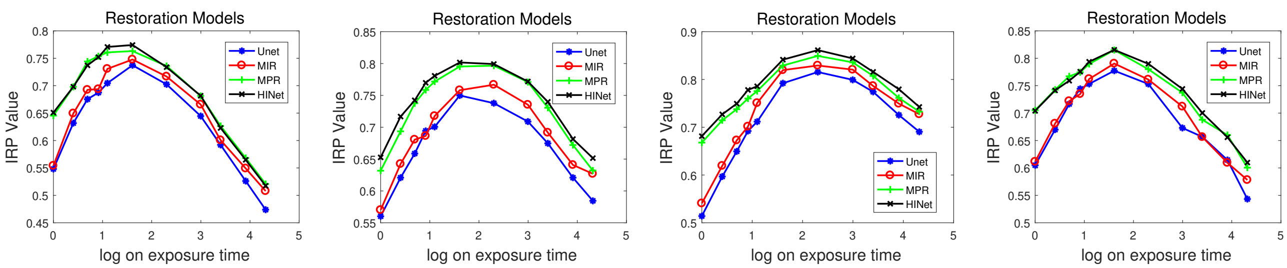

Figure 2. IRP values and their relationships generated by four restoration algorithms under different scenes.

1.3. Collected Data in the DS-IRP dataset

In Figure 3, we show example images contained in the established DS-IRP dataset and their corresponding IRP labels for a direct visualization.

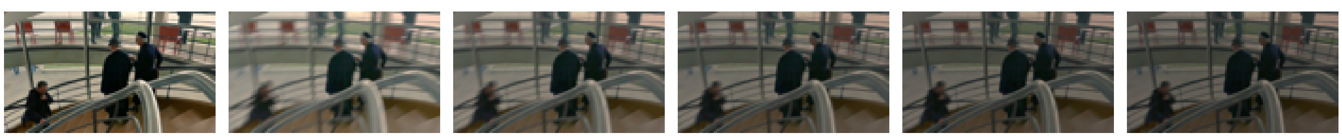

(a) gt (b) 0.4203 (c) 0.5357 (d) 0.6051 (e) 0.6343 (f) 0.6762

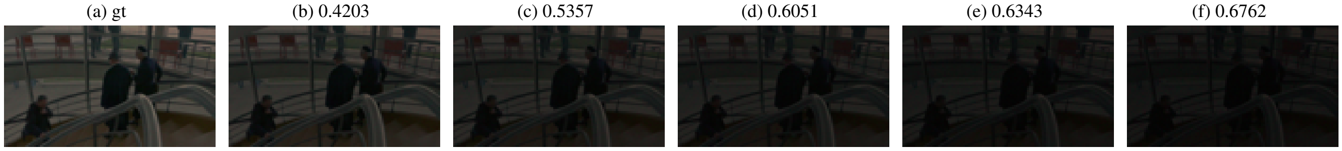

(g) 0.7595 (h) 0.7966 (i) 0.7749 (j) 0.7365 (k) 0.6915 (l) 0.6558

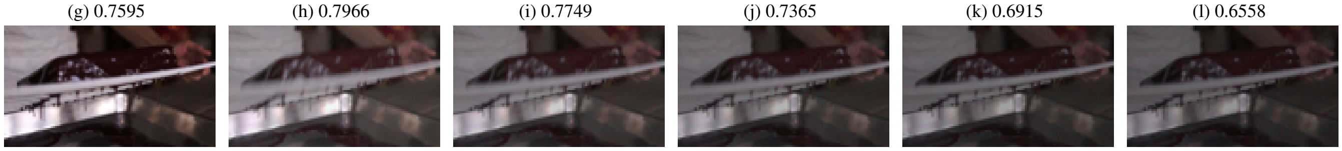

(m) gt (n) 0.5603 (o) 0.6566 (p) 0.7059 (q) 0.7449 (r) 0.7686

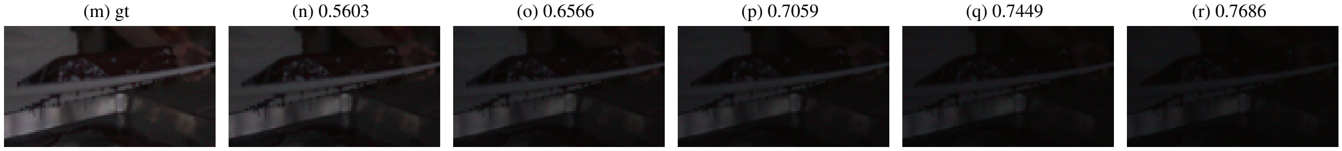

(s) 0.7942 (t) 0.7768 (u) 0.7170 (v) 0.6625 (w) 0.5966 (x) 0.5431

Figure 3. The IRP values of images with different ratios

In Figure 4, we also provide a histogram of the scene optical flow magnitudes in the DS-IRP dataset. The flows follow a log-Gaussian distribution similar to [6], and cover a wide range of motion magnitudes that might exist in real world scenarios.

2. Details for IRP Prediction Model

In this part, we show more model and implementation details.

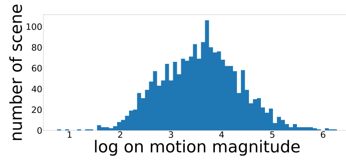

Figure 4. Histogram of the scene flow magnitudes in DS-IRP.

2.1. Selective Feature Fusion

The selective feature fusion operation is shown in Figure 5. After repeating the operation by three times, we sum over the three features, apply globally pooling and regress them to the final IRP score.

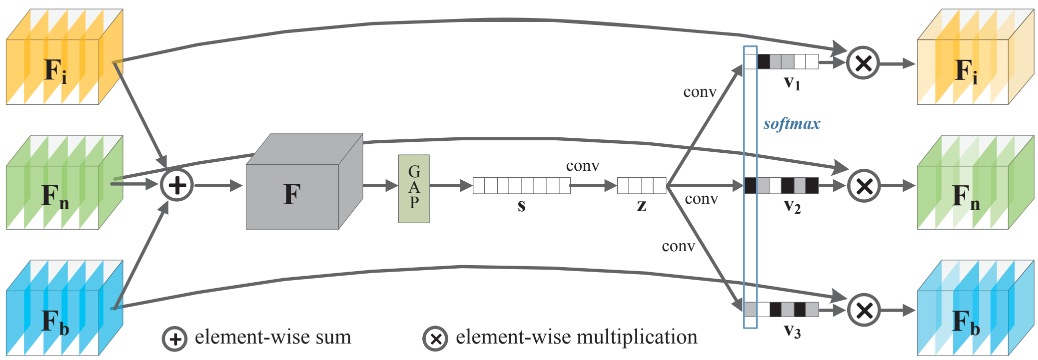

Figure 5. Figure illustration for the selective feature fusion operation.

2.2. Implementation Details

In our implementation, the channel number of feature maps $\mathbf{F_i}$, $\mathbf{F_n}$ and $\mathbf{F_b}$ are set to 512. The ASPP block [3] employs four parallel 3×3 convolutions with dilation 1, 2, 3 and 5, respectively. The squeeze ratio r in the selective feature fusion operation is set to 4, and the size of three layers in the MLP are set to 512, 256, 128, respectively.

During implementation, we built our model upon PyTorch and conducted the experiments on NVIDIA 1080Ti GPUs. The model receives input images with size 256×448, and batch size is set to 16. We train our model 30 epochs, with learning rate 1×10^{-4} dividing 10 every 10 epochs for convergence, and use Adam optimizer for training the model.

3. More Results on IRP Applications

3.1. Auxiliary Guidance for Restoration Models

In the main paper, we tested IRP as an auxiliary guidance to improve the image denoising model CBDnet. In this part, we present more experimental results on how IRP improves other image restoration models, including MIR [7], MPR [8] and HInet [2]. The results are shown in Table 2. As can be seen, when provided with IRP guidance, model performances consistently improved, demonstrating the effectiveness of introducing IRP for restoration models.

Table 2. Performance comparison on IRP as an auxiliary guidance to improve varying image restoration models on the SIDD dataset.

PSNR	CBD base [4]	MIR [7]	MPR [8]	HInet [2]
Baseline	40.227	40.015	40.589	40.633
Baseline+IRP	**40.771**	**40.379**	**40.654**	**40.658**
SSIM	CBD base [4]	MIR [7]	MPR [8]	HInet [2]
Baseline	0.9793	0.9818	0.9809	0.9825
Baseline+IRP	**0.9821**	**0.9824**	**0.9813**	**0.9828**

In Figure 6, we also show more qualitative comparisons. It can be seen that compared with the baseline, model provided with extra IRP guidance leads to less artifacts and better visual quality in restored results.

3.2. Indicator for Optimizing Camera Settings

We further show more qualitative comparisons on IRP as an indicator for optimizing camera exposure settings. Still, we present originally captured images and their restored results, as shown in Figure 7. It is worth noting that for imaging results captured under different exposure settings, different types of restoration algorithms are required. For example, auto-exposure captured images require deblurring approaches, and IRP selected images require denoising and enhancement techniques. Despite the difference, we endeavored our best to restore both images, expecting the best restored quality can be presented under the challenging real world imaging scenarios. Still, the results showed obvious visual difference, demonstrating the potential usage of IRP as a camera setting indicator in real world imaging applications.

References

[1] Meng Chang, Huajun Feng, Zhihai Xu, and Qi Li. Low-light image restoration with short-and long-exposure raw pairs. *IEEE Transactions on Multimedia*, 2021. 1

[2] Liangyu Chen, Xin Lu, Jie Zhang, Xiaojie Chu, and Chengpeng Chen. Hinet: Half instance normalization network for image restoration. In *Proceedings of the IEEE/CVF Conference on Computer Vision and Pattern Recognition*, pages 182–192, 2021. 2, 3

[3] Liang-Chieh Chen, George Papandreou, Iasonas Kokkinos, Kevin Murphy, and Alan L Yuille. Deeplab: Semantic image segmentation with deep convolutional nets, atrous convolution, and fully connected crfs. *IEEE transactions on pattern analysis and machine intelligence*, 40(4):834–848, 2017. 3

[4] Shi Guo, Zifei Yan, Kai Zhang, Wangmeng Zuo, and Lei Zhang. Toward convolutional blind denoising of real photographs. In *Proceedings of the IEEE/CVF Conference on Computer Vision and Pattern Recognition*, pages 1712–1722, 2019. 3

[5] Olaf Ronneberger, Philipp Fischer, and Thomas Brox. U-net: Convolutional networks for biomedical image segmentation. In *International Conference on Medical image computing and computer-assisted intervention*, pages 234–241. Springer, 2015. 2

[6] Tianfan Xue, Baian Chen, Jiajun Wu, Donglai Wei, and William T Freeman. Video enhancement with task-oriented flow. *International Journal of Computer Vision*, 127(8):1106–1125, 2019. 2

[7] Syed Waqas Zamir, Aditya Arora, Salman Khan, Munawar Hayat, Fahad Shahbaz Khan, Ming-Hsuan Yang, and Ling Shao. Learning enriched features for real image restoration and enhancement. In *Computer Vision–ECCV 2020: 16th European Conference, Glasgow, UK, August 23–28, 2020, Proceedings, Part XXV 16*, pages 492–511. Springer, 2020. 2, 3

[8] Syed Waqas Zamir, Aditya Arora, Salman Khan, Munawar Hayat, Fahad Shahbaz Khan, Ming-Hsuan Yang, and Ling Shao. Multi-stage progressive image restoration. In *Proceedings of the IEEE/CVF Conference on Computer Vision and Pattern Recognition*, pages 14821–14831, 2021. 2, 3

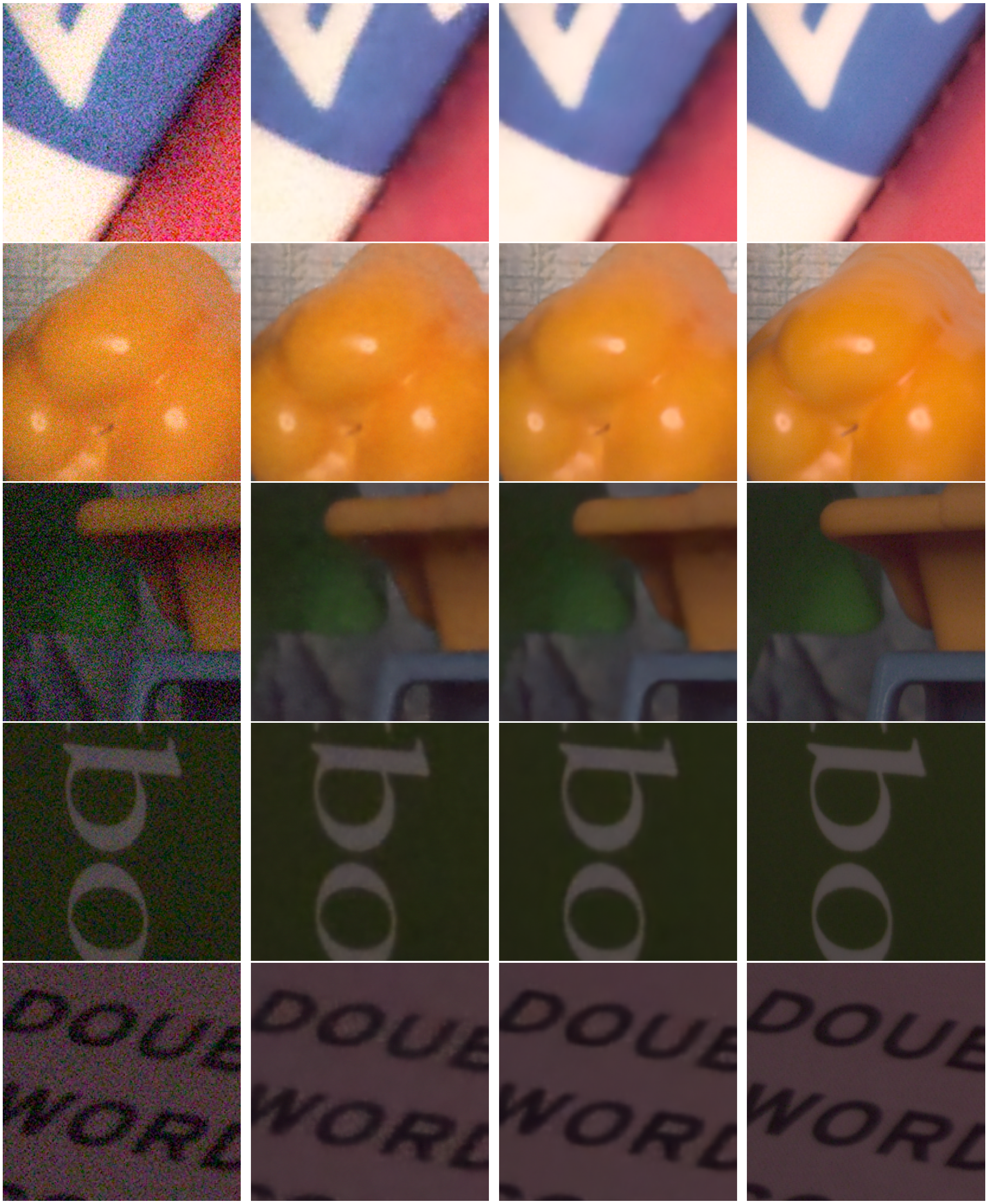

(a) Noisy (b) CDB baseline (c) CBD base+irp (d) gt

Figure 6. More qualitative comparisons of IRP as an auxiliary guidance on the denoising task.

(a) Auto-exposure (b) IRP-exposure (c) Auto-exposure restored (d) IRP-exposure restored

Figure 7. More comparisons of IRP for optimizing exposure settings against conventional auto-exposure settings of camera.